ARTICLES

Journal of Semiconductors
(2021) 42, 122002
doi: 10.1088/1674-4926/42/12/122002

Janus $MSiGeN_4$ (M = Zr and Hf) monolayers derived from centrosymmetric β-MA_2Z_4: A first-principles study

Xiaoshu Guo[1] and Sandong Guo[2, †]

[1]Xi'an University of Posts and Telecommunications, Xi'an 710121, China

[2]School of Electronic Engineering, Xi'an University of Posts and Telecommunications, Xi'an 710121, China

Abstract: A two-dimensional (2D) MA_2Z_4 family with α and β phases has been attracting tremendous interest, the $MoSi_2N_4$ and WSi_2N_4 of which have been successfully fabricated (Science 369, 670 (2020)). Janus monolayers have been achieved in many 2D families, so it is interesting to construct a Janus monolayer from the MA_2Z_4 family. In this work, Janus $MSiGeN_4$ (M = Zr and Hf) monolayers are predicted from β-MA_2Z_4, which exhibit dynamic, mechanical and thermal stabilities. It is found that they are indirect band-gap semiconductors by using generalized gradient approximation (GGA) plus spin-orbit coupling (SOC). With biaxial strain a/a_0 from 0.90 to 1.10, the energy band gap shows a nonmonotonic behavior due to a change of conduction band minimum (CBM). A semiconductor to metal transition can be induced by both compressive and tensile strains, and the phase transformation point is about 0.96 for compressive strain and 1.10 for tensile strain. The tensile strain can change the positions of CBM and valence band maximum (VBM), and can also induce the weak Rashba-type spin splitting near CBM. For $MSiGeN_4$ (M = Zr and Hf) monolayers, both an in-plane and out-of-plane piezoelectric response can be produced, when a uniaxial strain in the basal plane is applied, which reveals the potential as piezoelectric 2D materials. The high absorption coefficients in the visible light region suggest that $MSiGeN_4$ (M = Zr and Hf) monolayers have potential photocatalytic applications. Our works provide an idea to achieve a Janus structure from the MA_2Z_4 family, and can hopefully inspire further research exploring Janus MA_2Z_4 monolayers.

Key words: Janus monolayers; piezoelectronics; MA_2Z_4 family

Citation: X S Guo and S D Guo, Janus $MSiGeN_4$ (M = Zr and Hf) monolayers derived from centrosymmetric β-MA_2Z_4: A first-principles study[J]. *J. Semicond.*, 2021, 42(12), 122002. http://doi.org/10.1088/1674-4926/42/12/122002

1. Introduction

Janus 2D monolayers have currently attracted increasing attention, which possess unique physical and chemical properties caused by their special crystal structure, such as strong Rashba spin splitting, the second harmonic generation response, and out-of-plane piezoelectric polarizations[1]. Experimentally, Janus monolayer MoSSe, which is constructed from MoS_2/$MoSe_2$, has been achieved by different experimental methods with an out-of-plane structural asymmetry[2, 3]. In theory, many Janus 2D materials have been predicted by the first-principle calculations[4–12], such as Janus transition metal chalcogenides (TMDs), Janus transition-metal oxides, PtSSe, Janus MA_2Z_4, TiXY (X/Y = S, Se and Te), VSSe, SnSSe and Janus group-III monochalcogenide M_2XY (M = Ga, In; X/Y = S, Se and Te). Some unique properties have also been predicted, such as an out-of-plane piezoelectric coefficient[13, 14] and a significant Rashba spin splitting induced by intrinsic out-of-plane built-in electric field[10]. The Janus monolayer BiN and AsP field-effect transistors (FETs) possess sufficient competitiveness against other 2D FETs, which is confirmed by the benchmarking of the energy-delay product[15, 16].

Recently, the high-quality 2D $MoSi_2N_4$ and WSi_2N_4 are successfully synthesized with excellent ambient stability by chemical vapor deposition (CVD)[17], which starts a new 2D material family. In the wake of $MoSi_2N_4$ and WSi_2N_4, twelve kinds of 2D family WSi_2N_4 are proposed with α_i and β_i (i = 1 to 6) phases by intercalating MoS_2-type MZ_2 monolayer into InSe-type A_2Z_2 monolayer[18]. The MA_2Z_4 with 32 or 34 valence electrons (VEC) are mostly semiconductors. Moreover, α_2-WSi_2P_4 for the spin-valley polarization, α_1-$TaSi_2N_4$ for Ising superconductor and β_2-$SrGa_2Se_4$ for topological insulator are predicted[18]. And then, spin-valley polarization are also investigated in $MoSi_2N_4$, WSi_2N_4 and $MoSi_2As_4$[19, 20]. Intrinsic piezoelectricity of the MA_2Z_4 family along structure effect has been predicted by the first-principle calculations[21, 22]. Coexistence of intrinsic piezoelectricity and ferromagnetism induced by small biaxial strain in the septuple-atomic-layer VSi_2P_4 and VSi_2N_4 has been achieved, which offers the opportunities for achieving multifunctional electronic devices[23]. 2D van der Waals electrical contact to monolayer $MoSi_2N_4$ has been reported[24]. For example, the $MoSi_2N_4$/NbS_2 contact exhibits an ultralow Schottky barrier height[24]. High intrinsic lattice thermal conductivity in monolayer $MoSi_2N_4$ has also been predicted by solving the phonon Boltzmann transport equation[25].

It is very worthy of intensive study to construct a Janus monolayer from the MA_2Z_4 family. In our previous work, Janus $MSiGeN_4$ (M = Mo and W) monolayers have been predicted from α_1-MA_2Z_4[12]. The MSi_2N_4 and MGe_2N_4 (M = Zr and Hf) monolayers with a β_2 phase are semiconductors[18]. And then, in this work, Janus monolayer $MSiGeN_4$ (M = Zr and Hf)

Correspondence to: S D Guo, guosd@cumt.edu.cn
Received 10 JUNE 2021; Revised 21 JULY 2021.

Table 1. For the $ZrSiGeN_4$ ($HfSiGeN_4$) monolayer, the lattice constants a_0; the physical quantities associated with elasticity (the elastic constants C_{ij}, shear modulus G_{2D}, Young's modulus C_{2D} and Poisson's ratio ν); the gaps without/with SOC.

Parameter	Value
a_0 (Å)	3.110 (3.097)
C_{11}	403.92 (465.93)
C_{12} (N/m)	110.58 (135.19)
G_{2D}	146.67 (165.37)
C_{2D} (N/m)	373.65 (426.71)
ν	0.274 (0.290)
Gap (eV)	1.134 (1.336)
Gap-SOC (eV)	1.115 (1.282)

are built by replacing the Si/Ge atoms of the top SiN/GeN bilayer in a MSi_2N_4/MGe_2N_4 monolayer with Ge/Si atoms. Their crystal stability, electronic structures, piezoelectric and optical properties are investigated by the first-principle calculations. Calculated results show that $MSiGeN_4$ (M = Mo and W) monolayers are indirect gap semiconductors with dynamic, mechanical and thermal stabilities, and that tensile strain can induce weak Rashba-type spin splitting near CBM, and that $MSiGeN_4$ (M = Mo and W) monolayers have observable piezoelectric response and high absorption coefficients in the visible light region.

2. Computational detail

Within the density functional theory (DFT)[26], the projected augmented wave (PAW) method and GGA with the Perdew–Burke–Ernzerh (GGA-PBE) as the exchange-correlation functional are used, as implemented in the VASP code[27–30]. It has been proved that GGA is more suitable for a gap of experimentally synthesized $MoSi_2N_4$ monolayer than HSE06[17]. So, we use GGA to study the electronic and optical properties of $MSiGeN_4$ (M = Zr and Hf) monolayers. The SOC is included to investigate electronic structures of $MSiGeN_4$ (M = Zr and Hf) monolayers. The plane-wave cutoff energy of 500 eV is used with a 16 × 16 × 1 k-mesh. We relax both the lattice constants and internal atomic positions until the maximal residual Hellmann–Feynman forces are less than 0.0001 eV/Å. We use the total energy as convergence criterion, which is set to 10^{-8} eV. A vacuum space of larger than 30 Å is used to avoid interactions with other neighboring layers. After optimizing the crystal structure, 0.0001 eV/Å. We use the total energy as convergence criterion, which is set to with a supercell of 5 × 5 × 1, and the phonon dispersions of $MSiGeN_4$ (M = Zr and Hf) monolayers are calculated by using the PHONOPY code[31]. The ab-initio molecular dynamics (AIMD) simulations are performed with a supercell of size 4 × 4 × 1 for more than 3000 fs with a time step of 1 fs. The in-plane spin-textures are computed by using PYPROCAR code[32].

The elastic stiffness tensor C_{ij} are calculated by using strain-stress relationship (SSR), and the piezoelectric stress coefficients e_{ij} are attained by density functional perturbation theory (DFPT) method[33]. A Monkhorst–Pack mesh of 16 × 16 × 1 is used to calculate C_{ij}, and 9 × 16 × 1 for e_{ij}. Due to 3D periodic boundary conditions, the 2D elastic coefficients C_{ij}^{2D} and piezoelectric stress coefficients e_{ij}^{2D} have been

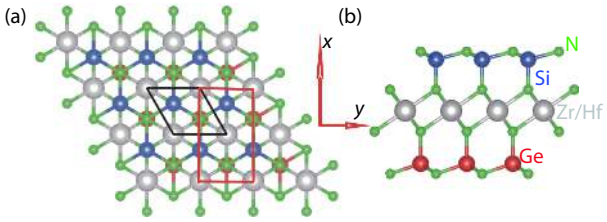

Fig. 1. (Color online) The crystal structures of $MSiGeN_4$ (M = Zr and Hf) monolayers: (a) top view and (b) side view.

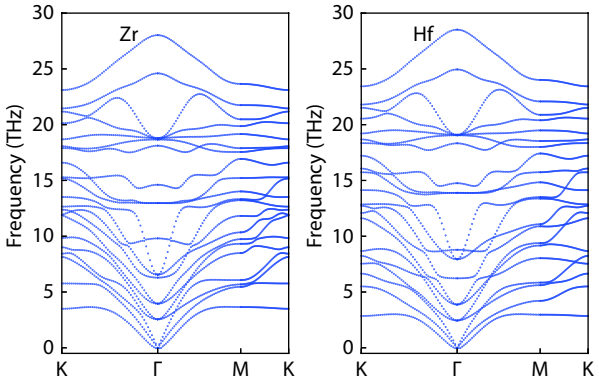

Fig. 2. (Color online)The phonon dispersion curves of $MSiGeN_4$ (M = Zr and Hf) monolayers with GGA.

renormalized: $C_{ij}^{2D} = L_z C_{ij}^{3D}$ and $e_{ij}^{2D} = L_z e_{ij}^{3D}$, where L_z is the length of the unit cell along the z direction. It is noted that the calculated optical properties also depend on L_z[34], which should be normalized by multiplying L_z/d, where d for the thickness of 2D material. However, the d is not well defined like graphene. In this work, the L_z = 35.8 Å is used as d.

3. Structure and stability

The crystal structure of the Janus monolayer $MSiGeN_4$ (M = Zr and Hf) is shown in Fig. 1 with the rhombus primitive cell and the rectangle supercell marked by black and red frames. With MN_2 (M = Zr and Hf) triple layers sandwiched between the SiN and GeN bilayers, the symmetry of Janus monolayer $MSiGeN_4$ (M = Zr and Hf) is lower than that of the MSi_2N_4 (M = Zr and Hf) or the MGe_2N_4 (M = Zr and Hf) monolayer due to the lack of the vertical reflection symmetry. In other words, Janus monolayer $MSiGeN_4$ (M = Zr and Hf) can be built by replacing the Si/Ge atoms of the top SiN/GeN bilayer in the MSi_2N_4/MGe_2N_4 monolayer with Ge/Si atoms. We use GGA to optimize lattice constants of monolayer $MSiGeN_4$ (M = Zr and Hf), and they are 3.110 and 3.097 Å, which are between the ones of MSi_2N_4 (3.05 and 3.19 Å) and MGe_2N_4 (3.04 and 3.18 Å)[18].

The dynamical stability of monolayer $MSiGeN_4$ (M = Zr and Hf) is studied by calculating their phonon band dispersions, which are shown in Fig. 2. It is clearly seen that the phonon branches are free from any imaginary frequencies, indicating the dynamical stability of these monolayers. They exhibit three acoustic and eighteen optical phonon branches due to seven atoms in the unit cell. In addition, the thermal stability is examined by AIMD simulations. During the simulations, the temperature is kept at 600 K, and the temperature and total energy fluctuations of only $ZrSiGeN_4$ monolayer are plotted in Fig. 3 due to similar results between $ZrSiGeN_4$ and $HfSiGeN_4$. The crystal structures of $ZrSiGeN_4$ at 600 K after the

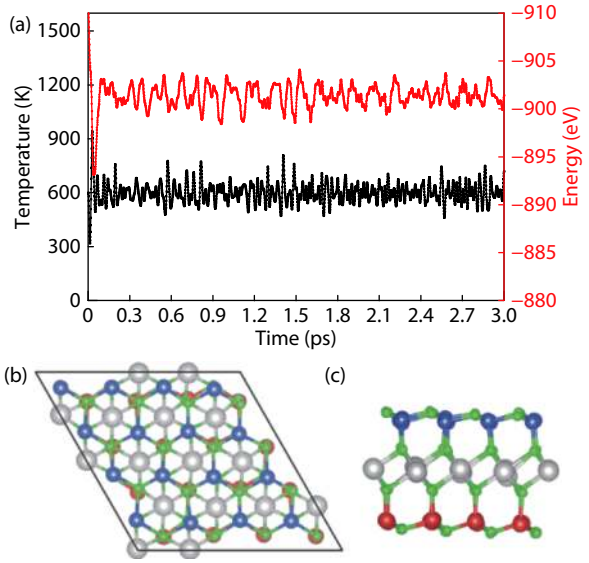

Fig. 3. (Color online) (a) The fluctuations of temperature and total energy with the time obtained from MD simulation of $ZrSiGeN_4$ monolayer at 600 K. (b, c) The snapshot of $ZrSiGeN_4$ monolayer at the end of MD simulation at 600 K ((b): Top views, (c): Side views).

simulation for 3 ps are also plotted in Fig. 3. It is found that monolayer $ZrSiGeN_4$ undergoes no structural reconstruction around 600 K, which indicates the thermal stability of these monolayers with the temperature and total energy fluctuating in the acceptable range.

To verify the mechanical stability of $MSiGeN_4$ (M = Zr and Hf), the investigation of the mechanical properties are carried out. Due to hexagonal symmetry, using Voigt notation, the elastic tensor can be expressed as:

$$C = \begin{pmatrix} C_{11} & C_{12} & 0 \\ C_{12} & C_{11} & 0 \\ 0 & 0 & (C_{11}-C_{12})/2 \end{pmatrix}. \quad (1)$$

The two independent elastic constants of $ZrSiGeN_4$/$HfSiGeN_4$ are C_{11} = 403.92/465.93 N/m and C_{12} = 110.58/135.19 N/m, and the $C_{66} = (C_{11} - C_{12})/2$ = 146.67 /165.37 N/m as shear modulus G_{2D}, which satisfy the Born criteria of mechanical stability[35]:

$$C_{11} > 0, \quad C_{66} > 0. \quad (2)$$

The 2D Young's moduli C_{2D} is given[35]:

$$C_{2D} = \frac{C_{11}^2 - C_{12}^2}{C_{11}}. \quad (3)$$

The calculated C_{2D} is 373.65/426.71 N/m for monolayer $ZrSiGeN_4$/$HfSiGeN_4$, which are larger than ones of many 2D materials[13, 36–38], indicating that these monolayers are rigid. However, they are smaller than ones of our predicted $MSiGeN_4$ (M = Mo and W) monolayers[12]. The Poisson's ratio ν is also calculated by C_{12}/C_{11}, and they are 0.274/0.290 for monolayer $ZrSiGeN_4$/$HfSiGeN_4$.

The MGe_2N_4 (M = Zr and Hf) has a lower formation energy than MSi_2N_4[18]. So, we calculate the cohesive energy (E_{coh}) of $MSiGeN_4$ with respect to MGe_2N_4, which is defined as $E_{coh} = E_{MSiGeN_4} - E_{Si} + E_{Ge} - E_{MGe_2N_4}$, where E_{MSiGeN_4} and $E_{MGe_2N_4}$ are the energies of the $MSiGeN_4$ and MGe_2N_4 monolayers, and E_{Si} and E_{Ge} are the energies of the isolated atoms of Si and Ge. The calculated E_{coh} is −1.85 eV/−1.90 eV for

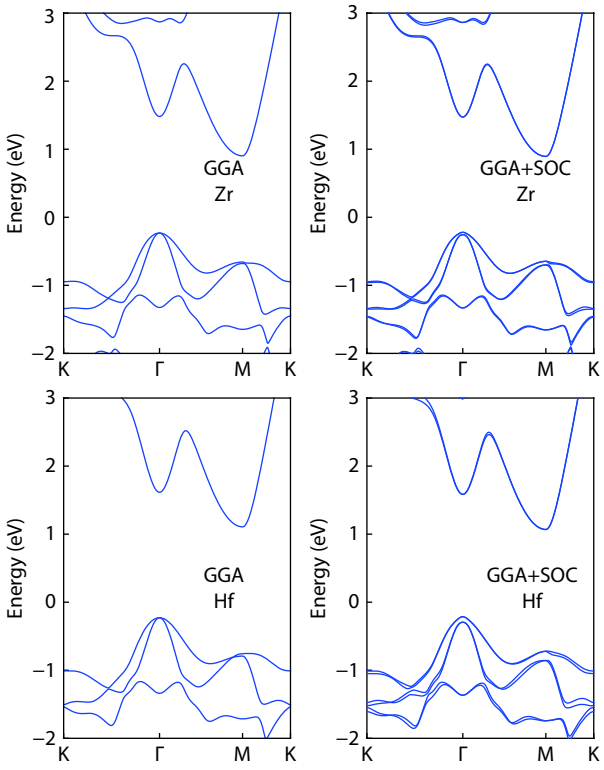

Fig. 4. (Color online) Band structures of $MSiGeN_4$ (M = Zr and Hf) monolayers without/with SOC (GGA/GGA+SOC).

$ZrSiGeN_4$/$HfSiGeN_4$ monolayer, which implies the feasibility of the experimental synthesis.

Phonon band dispersion calculations, elastic constants and AIMD simulations reveal the dynamical, mechanical and thermal stabilities of predicted monolayers. Monolayer MSi_2N_4 (M = Mo and W) have been synthesized by introducing Si during CVD growth of M_2N (M = Mo and W)[17]. We have proposed that the $MSiGeN_4$ (M = Mo and W) monolayers can be achieved by introducing Si and Ge during CVD growth of M_2N (M = Mo and W)[12]. The same way may be used to achieve the $MSiGeN_4$ (M = Zr and Hf) monolayers.

4. Electronic structure

For Janus $MSiGeN_4$ (M = Mo and W) monolayers, the SOC can produce important effects on their electronic structures, like Rashba spin splitting and valley polarization[12]. Thus, the SOC is considered to investigate electronic structures of $MSiGeN_4$ (M = Zr and Hf) monolayers, and the corresponding energy bands without/with SOC are shown in Fig. 4. The results without/with SOC show that $MSiGeN_4$ (M = Zr and Hf) monolayers are indirect gap semiconductors with VBM at the Γ point and CBM at the M point. The GGA gap of $ZrSiGeN_4$ is 1.134, and 1.336 eV for $HfSiGeN_4$. When including SOC, the gap of $ZrSiGeN_4$/$HfSiGeN_4$ reduces to 1.115 eV/1.282 eV. The SOC can also remove band degeneracy, and we take spin-orbit splitting (Δ) at VBM to illustrate the strength of SOC. The Δ is 35 meV/81 meV for $ZrSiGeN_4$/$HfSiGeN_4$, which means that the SOC has more strong effects on $HfSiGeN_4$.

Strain can be used to tune the physical and chemical properties of 2D materials[39–41]. Here, we examine the biaxial strain effects on the electronic properties of $MSiGeN_4$ (M = Zr and Hf) monolayers. The a/a_0 is used to simulate compressive/tensile strain with $a/a_0 < 1/a/a_0 > 1$, where a and a_0 are the

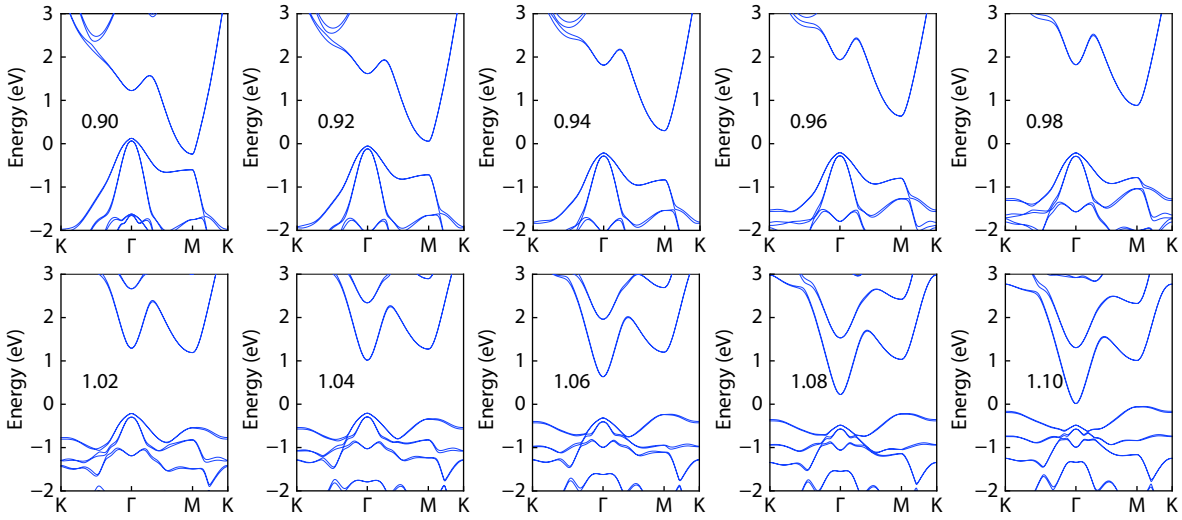

Fig. 5. (Color online) Band structures of $HfSiGeN_4$ monolayer with SOC (a/a_0 from 0.90 to 1.10).

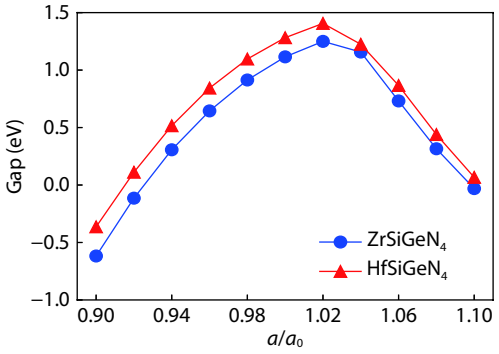

Fig. 6. (Color online) The band gaps of $MSiGeN_4$ (M = Zr and Hf) monolayers vs a/a_0 with SOC.

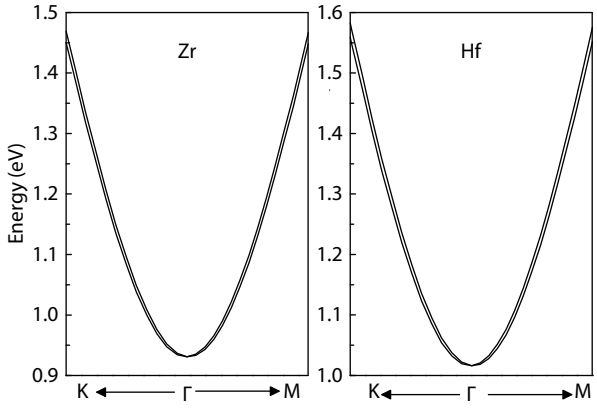

Fig. 7. The larger version around CBM for $MSiGeN_4$ (M = Zr and Hf) monolayers with SOC at 1.04 strain.

strained and unstrained lattice constants, respectively. Due to similar dependence on strain for electronic structures of $ZrSiGeN_4$ and $HfSiGeN_4$, we only show energy bands of $HfSiGeN_4$ as a function of a/a_0 in Fig. 5, and the the energy band gaps of $MSiGeN_4$ (M = Zr and Hf) monolayers with a/a_0 from 0.90 to 1.10 are plotted in Fig. 6. With strain from 0.90 to 1.10, the gap of monolayer $MSiGeN_4$ (M = Zr and Hf) firstly increases, and then decreases, which can be found in many 2D materials[12, 41]. In the considered strain range, it is found that both compressive and tensile strains can induce semiconductor to metal transition. The critical point is about 0.92 for compressive strain, and about 1.10 for tensile one. For $MSiGeN_4$ (M = Mo and W) monolayers, no semiconductor to metal transition is observed in the same strain range[12]. Another difference is that the maximum of gap can be induced by compressive strain for $MSiGeN_4$ (M = Mo and W)[12], and tensile strain for $MSiGeN_4$ (M = Zr and Hf).

It is found that tensile strain can tune the positions of VBM and CBM of $MSiGeN_4$ (M = Zr and Hf). Tensile strain can make CBM change from M point to Γ point, and VBM move from Γ point to one point along the M–K direction. These lead to that $MSiGeN_4$ (M = Zr and Hf) change from an indirect gap semiconductor to a direct one to an indirect one. For example, a direct gap semiconductor can be observed at 1.04 strain. The Rashba-type spin splitting near the CBM can be induced by tensile strain. At 1.04 strain, the enlarged views of the conduction bands near the Fermi level for $MSiGeN_4$ (M = Zr and Hf) monolayers using GGA+SOC are plotted in Fig. 7. It is clearly seen that a very weak Rashba-type spin splitting is produced. The constant energy 2D contour plots of spin texture of $HfSiGeN_4$ as a representative centered at the Γ point are plotted in Fig. 8 at an energy surface of 1.5 eV above the Fermi level. The spin-up (red) and spin-down (blue) electronic bands can be distinctly observed, which shows the Rashba-type spin splitting. Due to the pure 2D Rashba spin splitting, the concentric spin-texture circles are observed. In the Rashba spin split bands, the only in-plane S_X and S_Y spin components are observed with the lack of out-of-plane S_Z component. The tensile strain can tune the relative positions of valence band extrema (VBE), and can induce valence bands convergence, for example at a/a_0 = 1.06 point, which can produce an important influence on their electronic transport properties. However, the compressive strain produces small changes on electronic structures of $MSiGeN_4$ (M = Zr and Hf) monolayers except for the energy band gap.

5. Piezoelectric properties

The β-MSi_2N_4 or MGe_2N_4 (M = Zr and Hf) monolayers (No. 164) are centrosymmetric, which show no piezoelectricity. The $MSiGeN_4$ (M = Zr and Hf) monolayers (No. 156) lack inversion symmetry, and a reflection symmetry with respect to the central M atomic layer is broken. This leads to both e_{11}/d_{11} and

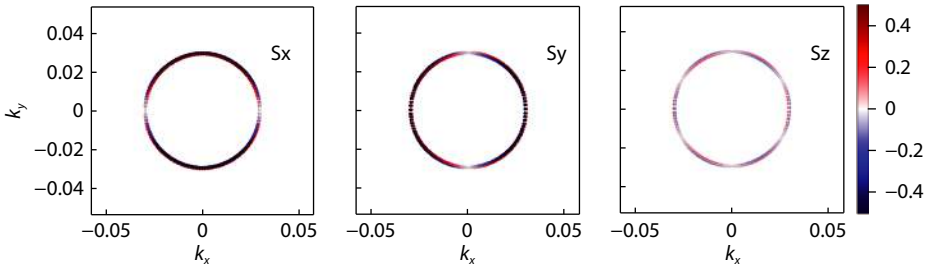

Fig. 8. (Color online) In-plane spin textures calculated at the iso-energy surface of 1.5 eV above the Fermi level for $HfSiGeN_4$ monolayer with red/blue colours being spin-up/spin-down states.

Table 2. Piezoelectric Coefficients e_{11}/e_{31} (10^{-10} C/m) and d_{11}/d_{31} (pm/V) of β-$MSiGeN_4$ (M = Zr and Hf) and α-$MSiGeN_4$ (M = Mo and W) monolayers.

$MSiGeN_4$	e_{11}	d_{11}	e_{31}	d_{31}
Zr	2.950	1.006	0.094	0.018
Hf	2.251	0.680	0.068	0.011
Mo	5.116	1.494	−0.087	−0.014
W	3.790	1.050	0.073	0.011

e_{31}/d_{31} being nonzero, and the piezoelectric stress and strain tensors become:

$$e = \begin{pmatrix} e_{11} & -e_{11} & 0 \\ 0 & 0 & -e_{11} \\ e_{31} & e_{31} & 0 \end{pmatrix}, \tag{4}$$

$$d = \begin{pmatrix} d_{11} & -d_{11} & 0 \\ 0 & 0 & -2d_{11} \\ d_{31} & d_{31} & 0 \end{pmatrix}. \tag{5}$$

For $MSiGeN_4$ (M = Mo and W) monolayers, the same reduced piezoelectric stress and strain tensors can be attained[12], but the original α-MSi_2N_4 or MGe_2N_4 (M = Mo and W) monolayers (No.187) lack inversion symmetry, and have vertical reflection symmetry, which gives rise to only in-plane piezoelectricity e_{11}/d_{11}. The two independent d_{11} and d_{31} are derived by $e_{ik} = d_{ij}C_{jk}$:

$$d_{11} = \frac{e_{11}}{C_{11} - C_{12}}, \quad d_{31} = \frac{e_{31}}{C_{11} + C_{12}}. \tag{6}$$

We use nonprimitive orthorhombic supercells as the computational unit cell (in Fig. 1) to calculate the e_{ij} of $MSiGeN_4$ (M = Zr and Hf) monolayers. Based on Eq. (6), their d_{ij} can be attained from previous calculated C_{ij} and e_{ij}. The calculated e_{ij} and d_{ij} of $MSiGeN_4$ (M = Zr and Hf) monolayers are listed in Table 2, along with ones of $MSiGeN_4$ (M = Mo and W) monolayers[12]. Calculated results show that the e_{11}/d_{11} of β-$MSiGeN_4$ (M = Zr and Hf) are lower than ones of α-$MSiGeN_4$ (M = Mo and W). Similar results can be found in Janus monolayer SnSSe and MoSSe[5]. The monolayer SnSSe is built from centrosymmetric monolayer SnS_2 or $SnSe_2$, while MoSSe can be attained from noncentrosymmetric MoS_2 or $MoSe_2$. And, the calculated e_{11}/d_{11} of SnSSe is lower than ones of MoSSe[5]. However, for both $MSiGeN_4$ (M = Zr and Hf) and $MSiGeN_4$ (M = Mo and W), their d_{31} are very small.

6. Optical properties

By calculating the complex dielectric function $\varepsilon(\omega)$ of $MSiGeN_4$ (M = Mo and W) monolayers, their optical properties can be attained. The imaginary part $\varepsilon_2(\omega)$ of $\varepsilon(\omega)$ is determined by a summation over empty band states as follows[42]:

$$\varepsilon_2(\omega) = \frac{2\pi e^2}{\Omega\varepsilon_0} \sum_{k,v,c} \delta(E_k^c - E_k^v - \hbar\omega) | < \psi_k^c | u.r | \psi_k^v > |^2, \tag{7}$$

where the vacuum dielectric constant, the volume and the energy of the incident phonon are marked by ε_0, Ω and $\hbar\omega$; The $u.r$ and ψ_k represent the momentum operator and the wave function at the k point; The v, c and u mean the valence bands, conduction bands and the polarization vector in the incident electric field. By the Kramers–Kronig relation, the real part $\varepsilon_1(\omega)$ can be calculated. According to the calculated $\varepsilon_1(\omega)$ and $\varepsilon_2(\omega)$, the absorption coefficient $\alpha(\omega)$ can be expressed as[43]:

$$\alpha(\omega) = \frac{\sqrt{2}\omega}{c} \left\{ \left[\varepsilon_1^2(\omega) + \varepsilon_2^2(\omega) \right]^{1/2} - \varepsilon_1(\omega) \right\}^{\frac{1}{2}}. \tag{8}$$

Here, the rhombus primitive cell is used to calculate the optical properties of $MSiGeN_4$ (M = Mo and W) monolayers. It is well known that the unit-cell volume Ω of a 2D material is not well-defined, which leads to some calculated physical properties of a 2D material depending on the the length of the unit cell along the z direction, for example optical properties[34]. The $\varepsilon(\omega)$ and $\alpha(\omega)$ of $MSiGeN_4$ (M = Mo and W) monolayers are calculated along xx/yy and zz directions, and are shown in Figs. 9 and 10. Because of hexagonal symmetry, the optical spectra between x and y directions are isotropic for light polarization along the in-plane directions. Due to similar energy band structures, it is clearly seen that the $ZrSiGeN_4$ and $HfSiGeN_4$ show very similar optical spectra. Due to distinct optical selection rules, there is a strong anisotropy in the optical spectra along xx/yy and zz directions. The static dielectric constants for $ZrSiGeN_4/HfSiGeN_4$ are 2.94/2.74 along xx/yy direction and 2.74/2.56 along zz direction, which can be attained from the real part of the dielectric constant at zero energy. It is found that a sharp increase for $\varepsilon_2(\omega)$ at the first onset of the optical transitions between xx/yy and zz directions is almost the same, and is at about 1.31 eV/1.71 eV for $ZrSiGeN_4/HfSiGeN_4$. From the ultraviolet to the visible light region, the calculated results imply that both xx/yy and zz directions show strong absorption intensity with the absorption coefficient values being more than 10^4 cm^{-1} in the visible region, which means high efficiency in the utilization of solar energy. It is found that the absorption intensity along the xx/yy direction has more smaller changes than one along zz direction in the visible light region, especially for $ZrSiGeN_4$.

7. Discussions and conclusion

The Janus α_1-$MSiGeN_4$ (M = Mo and W) and β_2-$MSiGeN_4$

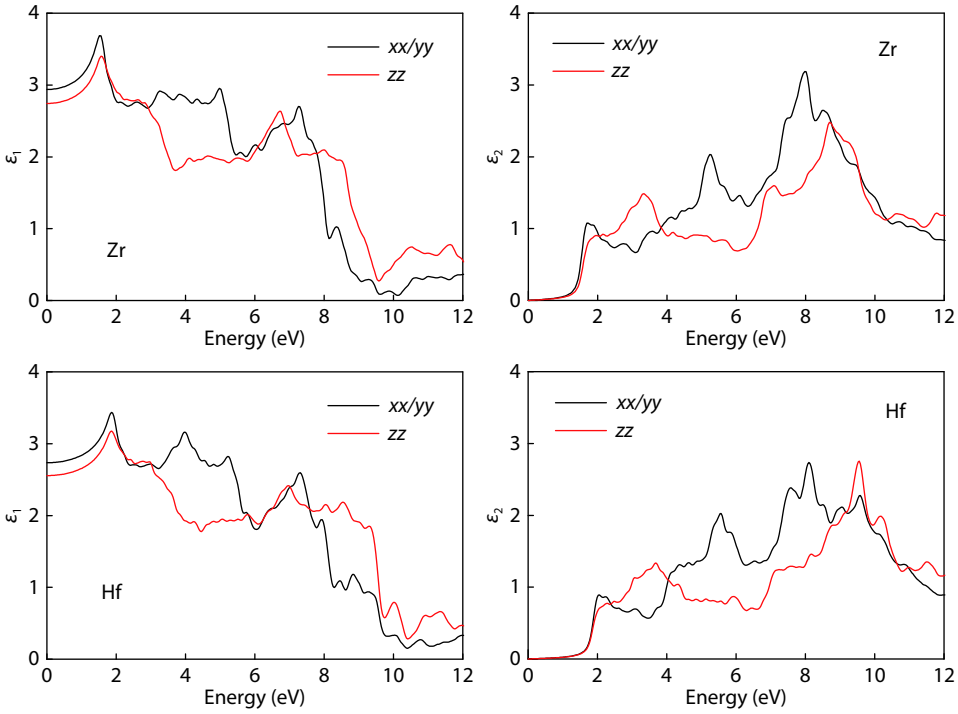

Fig. 9. (Color online) The calculated optical dielectric function of $MSiGeN_4$ (M = Zr and Hf) monolayers with real parts (Left) and imaginary parts (Right) along *xx*/*yy* and *zz* directions.

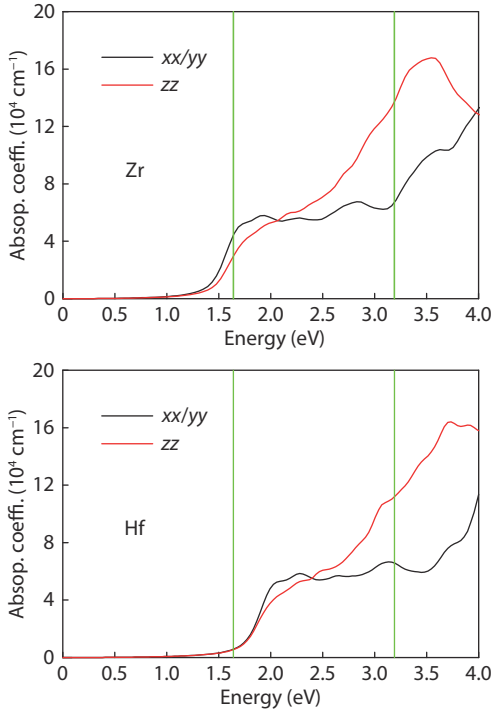

Fig. 10. (Color online) The optical absorption coefficients of $MSiGeN_4$ (M = Zr and Hf) monolayers along *xx*/*yy* and *zz* directions from 0 to 4 eV, and the visible light region (1.6–3.1 eV) is shown.

(M = Zr and Hf) monolayers have been predicted by the reliable first-principle calculations. In fact, our works provide an idea to achieve Janus structures from the MA_2Z_4 family, and many Janus MA_2Z_4 can be further investigated. For example, α_2-$MSiGeP_4$ (M = Cr, Mo and W) can be built, based on semiconducting MSi_2P_4 and MGe_2P_4 (M = Cr, Mo and W)[18]. In these Janus MA_2Z_4, both in-plane and out-of-plane piezoelectricity, Rashba-type spin splitting, valley polarization and second harmonic generation responses can be explored.

In summary, the electronic structures, piezoelectric properties and optical properties of Janus $MSiGeN_4$ (M = Zr and Hf) monolayers are systematically investigated by DFT. They exhibit mechanical, dynamic and thermal stabilities, and show indirect gap properties. It is found that strain can effectively tune their electronic structures, and can induce semiconductors to metal transition in the considered strain range. A very weak Rashba-type spin splitting near CBM can be induced by tensile strain. Both in-plane and out-of-plane piezoelectricity are predicted in $MSiGeN_4$ (M = Zr and Hf) monolayers. The high absorption coefficients in the visible light region can be found along both *xx*/*yy* and *zz* directions. Our works can stimulate further experimental works to synthesize Janus MA_2Z_4 monolayers, and will motivate farther theoretical studies of other Janus MA_2Z_4, like α_2-$MSiGeP_4$ (M = Cr, Mo and W) monolayers.

Acknowledgements

This work is supported by Natural Science Basis Research Plan in Shaanxi Province of China (2021JM-456). We are grateful to the Advanced Analysis and Computation Center of China University of Mining and Technology (CUMT) for the award of CPU hours and WIEN2k/VASP software to accomplish this work.

References

[1] Zhang L, Yang Z, Gong T, et al. Recent advances in emerging Janus two-dimensional materials: From fundamental physics to device applications. J Mater Chem A, 2020, 8, 8813

[2] Lu A Y, Zhu H Y, Xiao J, et al. Janus monolayers of transition metal dichalcogenides. Nat Nanotechnol, 2017, 12, 744

[3] Zhang J, Jia S, Kholmanov I, et al. Janus monolayer transition-metal dichalcogenides. ACS Nano, 2017, 11, 8192

[4] Singh S, Romero A H. Giant tunable Rashba spin splitting in a two-dimensional BiSb monolayer and in BiSb/AlN heterostructures. Phys Rev B, 2017, 95, 165444
[5] Guo S D, Guo X S, Han R Y, et al. Predicted Janus SnSSe monolayer: A comprehensive first-principles study. Phys Chem Chem Phys, 2019, 21, 24620
[6] Guo Y D, Zhang H B, Zeng H L, et al. A progressive metal–semiconductor transition in two-faced Janus monolayer transition-metal chalcogenides. Phys Chem Chem Phys, 2018, 20, 21113
[7] Peng R, Ma Y D, Huang B B, et al. Two-dimensional Janus PtSSe for photocatalytic water splitting under the visible or infrared light. J Mater Chem A, 2019, 7, 603
[8] Mogulkoc A, Mogulkoc Y, Jahangirov S, et al. Characterization and stability of Janus TiXY (X/Y = S, Se, and Te) monolayers. J Phys Chem C, 2019, 123, 29922
[9] Zhang C M, Nie Y H, Sanvito S, et al. First-principles prediction of a room-temperature ferromagnetic Janus VSSe monolayer with piezoelectricity, ferroelasticity, and large valley polarization. Nano Lett, 2019, 19, 1366
[10] Cheng Y C, Zhu Z Y, Tahir M, et al. Spin-orbit–induced spin splittings in polar transition metal dichalcogenide monolayers. EPL, 2013, 102, 57001
[11] Sun M L, Ren Q Q, Wang S K, et al. Electronic properties of Janus silicene: New direct band gap semiconductors. J Phys D, 2016, 49, 445305
[12] Guo S D, Mu W Q, Zhu Y T, et al. Predicted septuple-atomic-layer Janus $MSiGeN_4$ (M = Mo and W) monolayers with Rashba spin splitting and high electron carrier mobilities. J Mater Chem C, 2021, 9, 2464
[13] Dong L, Lou J, Shenoy V B. Large in-plane and vertical piezoelectricity in Janus transition metal dichalchogenides. ACS Nano, 2017, 11, 8242
[14] Yagmurcukardes M, Sevik C, Peeters F M. Electronic, vibrational, elastic, and piezoelectric properties of monolayer Janus MoSTe phases: A first-principles study. Phys Rev B, 2019, 100, 045415
[15] Zhou W H, Zhang S L, Guo S Y, et al. Designing sub-10-nm metal-oxide-semiconductor field-effect transistors via ballistic transport and disparate effective mass: The case of two-dimensional BiN. Phys Rev Appl, 2020, 13, 044066
[16] Zhou W H, Zhang S L, Wang Y Y, et al. Anisotropic in-plane ballistic transport in monolayer black arsenic- phosphorus FETs. Adv Electron Mater, 2020, 6, 1901281
[17] Hong Y L, Liu Z, Wang L, et al. Chemical vapor deposition of layered two-dimensional $MoSi_2N_4$ materials. Science, 2020, 369, 670
[18] Wang L, Shi Y P, Liu M F, et al. Intercalated architecture of MA_2Z_4 family layered van der Waals materials with emerging topological, magnetic and superconducting properties. Nat Commun, 2021, 12, 2361
[19] Li S, Wu W K, Feng X L, et al. Valley-dependent properties of monolayer $MoSi_2N_4$, WSi_2N_4, and $MoSi_2As_4$. Phys Rev B, 2020, 102, 235435
[20] Yang C, Song Z G, Sun X T, et al. Valley pseudospin in monolayer $MoSi_2N_4$ and $MoSi_2As_4$. Phys Rev B, 2021, 103, 035308
[21] Guo S D, Zhu Y T, Mu W Q, et al. Intrinsic piezoelectricity in monolayer MSi_2N_4 (M = Mo, W, Cr, Ti, Zr and Hf). EPL, 2020, 132, 57002
[22] Guo S D, Zhu Y T, Mu W Q, et al. Structure effect on intrinsic piezoelectricity in septuple-atomic-layer MSi_2N_4 (M = Mo and W). Comput Mater Sci, 2021, 188, 110223
[23] Guo S D, Mu W Q, Zhu Y T, et al. Coexistence of intrinsic piezoelectricity and ferromagnetism induced by small biaxial strain in septuple-atomic-layer VSi_2P_4. Phys Chem Chem Phys, 2020, 22, 28359
[24] Cao L M, Zhou G H, Wang Q Q, et al. Two-dimensional van der Waals electrical contact to monolayer $MoSi_2N_4$. Appl Phys Lett, 2021, 118, 013106
[25] Yu J H, Zhou J, Wan X G, et al. High intrinsic lattice thermal conductivity in monolayer $MoSi_2N_4$. New J Phys, 2021, 23, 033005
[26] Hohenberg P, Kohn W. Inhomogeneous electron gas. Phys Rev, 1964, 136, B864
[27] Kresse G. Ab initio molecular dynamics for liquid metals. J Non Cryst Solids, 1995, 192/193, 222
[28] Kresse G, Furthmüller J. Efficiency of ab-initio total energy calculations for metals and semiconductors using a plane-wave basis set. Comput Mater Sci, 1996, 6, 15
[29] Kresse G, Joubert D. From ultrasoft pseudopotentials to the projector augmented-wave method. Phys Rev B, 1999, 59, 1758
[30] Perdew J P, Burke K, Ernzerhof M. Generalized gradient approximation made simple. Phys Rev Lett, 1996, 77, 3865
[31] Togo A, Oba F, Tanaka I. First-principles calculations of the ferroelastic transition between rutile-type and $CaCl_2$-type SiO_2 at high pressures. Phys Rev B, 2008, 78, 134106
[32] Herath U, Tavadze P, He X, et al. P_yProcar: A Python library for electronic structure pre/post-processing. Comput Phys Commun, 2020, 251, 107080
[33] Wu X F, Vanderbilt D, Hamann D R. Systematic treatment of displacements, strains, and electric fields in density-functional perturbation theory. Phys Rev B, 2005, 72, 035105
[34] Guo G Y, Chu K C, Wang D S, et al. Linear and nonlinear optical properties of carbon nanotubes from first-principles calculations. Phys Rev B, 2004, 69, 205416
[35] Andrew R C, Mapasha R E, Ukpong A M, et al. Erratum: Mechanical properties of graphene and boronitrene [Phys. Rev. B 85, 125428 (2012)]. Phys Rev B, 2004, 69, 205416
[36] Blonsky M N, Zhuang H L, Singh A K, et al. Ab initio prediction of piezoelectricity in two-dimensional materials. ACS Nano, 2015, 9, 9885
[37] Fei R X, Li W B, Li J, et al. Giant piezoelectricity of monolayer group IV monochalcogenides: SnSe, SnS, GeSe, and GeS. Appl Phys Lett, 2015, 107, 173104
[38] Duerloo K A N, Ong M T, Reed E J. Intrinsic piezoelectricity in two-dimensional materials. J Phys Chem Lett, 2012, 3, 2871
[39] Fan Z Q, Jiang X W, Wei Z M, et al. Tunable electronic structures of GeSe nanosheets and nanoribbons. J Phys Chem C, 2017, 121, 14373
[40] Xue X X, Feng Y X, Liao L, et al. Strain tuning of electronic properties of various dimension elemental tellurium with broken screw symmetry. J Phys: Condens Matter, 2018, 30, 125001
[41] Guo S D, Dong J. Biaxial strain tuned electronic structures and power factor in Janus transition metal dichalchogenide monolayers. Semicond Sci Technol, 2018, 33, 085003
[42] Gajdoš M, Hummer K, Kresse G, et al. Linear optical properties in the projector-augmented wave methodology. Phys Rev B, 2006, 73, 045112
[43] Huang X, Paudel T R, Dong S, et al. Hexagonal rare-earth manganites as promising photovoltaics and light polarizers. Phys Rev B, 2015, 92, 125201

Xiaoshu Guo received his MS from Yanshan University in 2011. She is currently a junior engineer. Her research focuses on thermoelectricity, piezoelectricity and optical properties of 2D materials.

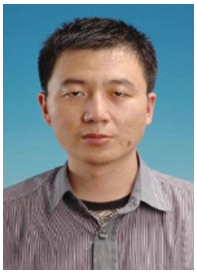

Sandong Guo received his PhD from Institute of Physics, Chinese Academy of Sciences in 2012. He is currently an Associate Professor. His research focuses on physical and chemical properties of 2D materials, such as thermoelectricity, piezoelectricity, topological properties and so on.